

Representing Cloud Mesoscale Variability in Superparameterized Climate Models

Jansson, F.R.; Van Den Oord, Gijs; Pelupessy, Inti; Chertova, Maria; Grönqvist, Johanna H.; Siebesma, A.P.; Crommelin, Daan

DOI

[10.1029/2021MS002892](https://doi.org/10.1029/2021MS002892)

Publication date

2022

Document Version

Final published version

Published in

Journal of Advances in Modeling Earth Systems

Citation (APA)

Jansson, F. R., Van Den Oord, G., Pelupessy, I., Chertova, M., Grönqvist, J. H., Siebesma, A. P., & Crommelin, D. (2022). Representing Cloud Mesoscale Variability in Superparameterized Climate Models. *Journal of Advances in Modeling Earth Systems*, 14(8), Article e2021MS002892. <https://doi.org/10.1029/2021MS002892>

Important note

To cite this publication, please use the final published version (if applicable). Please check the document version above.

Copyright

Other than for strictly personal use, it is not permitted to download, forward or distribute the text or part of it, without the consent of the author(s) and/or copyright holder(s), unless the work is under an open content license such as Creative Commons.

Takedown policy

Please contact us and provide details if you believe this document breaches copyrights. We will remove access to the work immediately and investigate your claim.



RESEARCH ARTICLE

10.1029/2021MS002892

Representing Cloud Mesoscale Variability in Superparameterized Climate Models

Fredrik Jansson^{1,2} , **Gijs van den Oord³** , **Inti Pelupessy³** , **Maria Chertova³**,
Johanna H. Grönqvist⁴ , **A. Pier Siebesma^{1,5}** , and **Daan Crommelin^{2,6}** 

¹Delft University of Technology, Delft, The Netherlands, ²Centrum Wiskunde & Informatica, Amsterdam, The Netherlands, ³Netherlands eScience Center, Amsterdam, The Netherlands, ⁴Department of Physics, Åbo Akademi University, Turku, Finland, ⁵Royal Netherlands Meteorological Institute, De Bilt, The Netherlands, ⁶Korteweg-de Vries Institute for Mathematics, University of Amsterdam, Amsterdam, The Netherlands

Key Points:

- Superparameterization (SP) in weather and climate models is used to improve the representation of clouds
- We show that SP suppresses the transport of clouds
- A scheme for controlling the humidity variation partially improves cloud representation in superparameterized models

Supporting Information:

Supporting Information may be found in the online version of this article.

Correspondence to:

F. Jansson,
fjansson@abo.fi

Citation:

Jansson, F., van den Oord, G., Pelupessy, I., Chertova, M., Grönqvist, J. H., Siebesma, A. P., & Crommelin, D. (2022). Representing cloud mesoscale variability in superparameterized climate models. *Journal of Advances in Modeling Earth Systems*, 14, e2021MS002892. <https://doi.org/10.1029/2021MS002892>

Received 8 NOV 2021
Accepted 9 JUL 2022

Author Contributions:

Conceptualization: Fredrik Jansson, Gijs van den Oord, A. Pier Siebesma, Daan Crommelin

Funding acquisition: A. Pier Siebesma, Daan Crommelin

Software: Fredrik Jansson, Gijs van den Oord, Inti Pelupessy, Maria Chertova

Visualization: Fredrik Jansson, Johanna H. Grönqvist

Writing – original draft: Fredrik Jansson, Johanna H. Grönqvist, A. Pier Siebesma

© 2022 The Authors. Journal of Advances in Modeling Earth Systems published by Wiley Periodicals LLC on behalf of American Geophysical Union. This is an open access article under the terms of the [Creative Commons Attribution-NonCommercial-NoDerivs License](https://creativecommons.org/licenses/by/4.0/), which permits use and distribution in any medium, provided the original work is properly cited, the use is non-commercial and no modifications or adaptations are made.

Abstract In atmospheric modeling, superparameterization (SP) has gained popularity as a technique to improve cloud and convection representations in large-scale models by coupling them locally to cloud-resolving models. We show how the different representations of cloud water in the local and the global models in SP lead to a suppression of cloud advection and ultimately to a systematic underrepresentation of the cloud amount in the large-scale model. We demonstrate this phenomenon in a regional SP experiment with the global model OpenIFS coupled to the local model Dutch Atmospheric Large Eddy Simulation, as well as in an idealized setup, where the large-scale model is replaced by a simple advection scheme. As a starting point for mitigating the problem of suppressed cloud advection, we propose a scheme where the spatial variability of the local model's total water content is enhanced in order to match the global model's cloud condensate amount. The proposed scheme enhances the cloud condensate amount in the test cases, however a large discrepancy remains, caused by rapid dissipation of the clouds added by the proposed scheme.

Plain Language Summary In this article, we investigate a technique called superparameterization (SP) for improving how global weather and climate models represent clouds and convection. In current operational global weather and climate models, the resolution is limited to 10–100 km by computational resources. This is not sufficient to resolve cloud and convective processes. The effect of these processes must then be approximated by so-called parameterizations. SP uses another, local atmospheric model with a higher resolution, nested inside the columns of the global model, to evaluate the effects of clouds and convection. By analyzing results from a superparameterized simulation, we show that SP as it is generally implemented suppresses advection of existing clouds from one grid column to another in the global model, leading to a severe underestimation of the amount of shallow clouds. The suppression occurs because the global and local models represent clouds in different ways, and the commonly used SP scheme does not communicate the full cloud information from the global model to the local one. Adding such a coupling of the cloud information to the SP scheme partially improves the advection of clouds. The remaining discrepancies indicate that there are still missing processes in the superparameterized representation of boundary layer clouds.

1. Introduction

Many of the systematic biases and uncertainties in conventional general circulation models (GCMs) can be attributed to the highly parameterized representation of clouds, turbulence and convection. It is even questionable whether these biases will be eliminated unless resolutions of GCMs become fine enough for these processes to be numerically resolved. As pointed out by Arakawa et al. (2011, 2016) there are essentially two possible routes toward such global large eddy models (GLEMs).

Route 1 follows the traditional approach of continuously refining the resolution until clouds, convection and turbulence are sufficiently resolved. This requires scale aware parameterizations for these processes that are gradually switched off with increasing resolution in a physically consistent manner. Alternatively one can make large jumps in the used resolution so certain parameterizations can be switched off abruptly. At present, a horizontal resolution of around 1 km is the highest possible resolution for subseasonal global simulations of the atmosphere (Satoh et al., 2019; Stevens, Satoh, et al., 2019). For such storm resolving resolutions, the general belief is that deep moist convective overturning is sufficiently well resolved to the extent that any additional deep convection

Writing – review & editing: Fredrik Jansson, Gijs van den Oord, Inti Pelupessy, Maria Chertova, Johanna H. Grönqvist, A. Pier Siebesma, Daan Crommelin

parameterization will deteriorate the skill of the simulation. Obviously, at these storm resolving resolutions there is still a turbulence parameterization required as well as some parameterized representation of boundary layer cloudiness and shallow cumulus convection.

Route 2 makes use of a “multi-scale modeling framework” (MMF). In its original form, deep moist convection parameterization was replaced (or “superparameterized”) by a 2D storm resolving model (2D SRM) in each cell of a GCM (Grabowski, 2001; Grabowski & Smolarkiewicz, 1999; Khairoutdinov et al., 2005; Randall et al., 2003; Tao et al., 2009). More recently, the use of a 3D large eddy model (LEM) as a superparameterization (SP) for clouds, convection and turbulence has been proposed (Grabowski, 2016; Jansson et al., 2019; Parishani et al., 2017). This approach has the advantage that most of the small scale dynamics and cloud microphysics is well represented while the GCM can still be formulated in an efficient hydrostatic manner. Further computational advantages of this approach over a GLEM are discussed in Grabowski (2016). Because the use of a 3D LEM as a SP on a global scale is computationally not yet feasible, Jansson et al. (2019) implemented the possibility of using a 3D LEM on a regional scale in the global Integrated Forecasting System (IFS) of the ECMWF (Malardel et al., 2016; Sparrow et al., 2021). This implies that a number of grid cells in the IFS can be selected to be superparameterized while the remaining part of the IFS will use the conventional parameterizations for clouds, convection and turbulence. In the study by Jansson et al. (2019) the implementation of the Dutch Atmospheric Large Eddy Simulation (DALES; Heus et al. (2010)) model as a SP into the IFS was documented, along with a case study of local shallow cumulus convection over land to demonstrate the potential of this approach.

Despite the many advantages, the MMF does not come without problems. One drawback of this approach is that the communication between LEMs embedded in neighboring GCM columns can only occur through the GCM, primarily through advection of the variables in the GCM. Therefore it is not possible in the superparameterized framework to advect a spatial structure, as resolved by a local LEM, to a neighboring GCM grid column—only the mean state of a GCM grid column can be advected to a neighboring column. In other words, compared to a global LEM, the MMF introduces a scale break as it does not allow structures, or even variability, to grow upscale to scales beyond the size of the GCM grid size. The same scale cutoff is naturally present in a GCM, where processes on scales smaller than the grid size are parameterized. SP should be viewed as an attempt for a better and model-informed parameterization, rather than a substitute for a global LEM. Chern et al. (2020) evaluates biases in the size of rain events simulated in the Goddard MMF, caused by the size constraint imposed by the cloud-resolving model. On the other hand, other phenomena such as mesoscale convective systems and tropical cyclones have been shown to be able to grow across the scales of the two models when simulated with SP (Lin et al., 2022; Pritchard et al., 2011; Tulich, 2015).

Another related but more severe drawback of the MMF follows from the fact that while most GCMs carry separate prognostic variables for the water vapor and the water in the condensed phase, this is not the case for the local LEM. Most local models use the total water specific humidity q_t , that is, the sum of water vapor and the condensed water, as a prognostic variable. This implies that while the GCM separately advects the amount of condensed water and water vapor from one grid cell to a neighboring one, the local LEM of the neighboring cell is incapable of digesting this information and can only take the sum of the advected vapor and condensed water as input.

As will be demonstrated in detail, this implies that a cloud which is advected to a neighboring grid column by the GCM will be directly diluted and dissipated in the local LEM of the neighboring column. This dissipation of advected subgrid clouds, such as cumulus types, is likely a general problem in all published studies of SPs that make use of SRMs with total water specific humidity as a prognostic variable. Marine shallow cumulus is an abundant cloud type, with important but not precisely known climate feedback properties (Bony & Dufresne, 2005; Bony et al., 2020).

In short, the main purpose of this paper is (a) to show that most SPs as they are used today dissipate most of the advected cloud condensate of sub-grid-scale clouds, leading to strong underestimation of cloud condensate and (b) to explore a simple solution by coupling the appropriate variance of humidity between GCM grid cells that are commensurate with the advected cloud condensate.

The paper is organized as follows. In Section 2, we analyze the SP procedure and its consequences for cloud advection. As an example, we show a regional SP simulation with the LEMs located over the subtropical Northern Atlantic Ocean, in the vicinity of Barbados. The example shows almost complete suppression of cloud

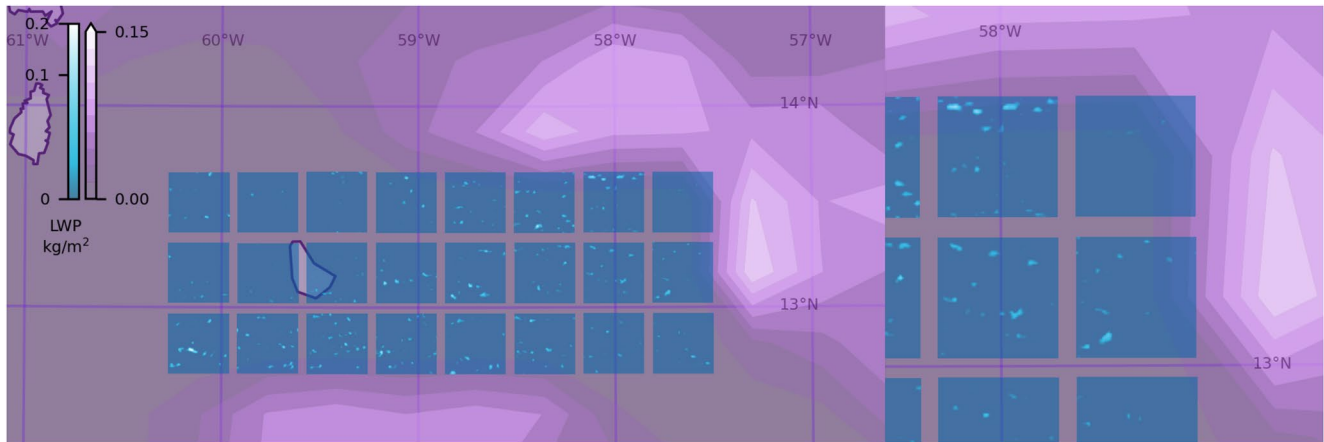


Figure 1. A superparameterized simulation over Barbados on 2013-12-15 at 9:30 UTC, showing that incoming clouds in the large-scale (purple) model do not easily advect into the superparameterized region (blue boxes). The right hand-image shows a magnification of the eastern (upwind) part of the superparameterization region.

advection into the superparameterized region. In Section 3, we propose an extension of the SP scheme with a procedure to adjust the small-scale variability in the local models, in order to better preserve the cloud condensate. In Section 4, we present an idealized SP experiment where the large-scale model consists of only advection, to demonstrate the lack of cloud advection in SP and to see the impact of the variability coupling scheme in a simple setup. The effects of the variability coupling procedure on the full Barbados simulation is evaluated in Section 5. In the concluding Section 6, we discuss the impact of the cloud advection issue on SP experiments.

2. Suppressed Cloud Advection in Superparameterization

In this section, we show that a SP scheme can lead to suppressed advection of cloud condensate in the large-scale model.

2.1. Superparameterized Barbados Experiment

We demonstrate this lack of cloud advection in an experiment with the regional SP of OpenIFS with DALES (Jansson et al., 2019), with the SP region located over Barbados, as shown in Figure 1. This case has a wind from the east which brings clouds into the superparameterized region. The IFS model, initialized from ERA5 as in Jansson et al. (2019), shows only shallow clouds entering the SP region, cloud base varies between 500 and 800 m, while the cloud top varies between 1.4 and 3 km during the simulation (this can be seen below in Figure 11 showing vertical profiles of cloud condensate in selected grid points). In the experiments shown here, IFS was operating at an effective horizontal resolution of 40 km (T511L91 grid). The DALES domains cover 12.8×12.8 km with a horizontal resolution of 200 m. The DALES domains are 5 km high, with a vertical resolution of 20 m. Further details are given in (Jansson et al., 2019). A satellite image of the same area is shown in Figure 2.

The region features persistent shallow cumulus clouds transported by the trade winds, with cloud patterns and cloud organizations occurring on widely different length scales. It is an interesting test case for SP, in particular to investigate how well SP represents cloud organization. The time and the location were chosen to coincide with the NARVAL (Stevens, Ament, et al., 2019) observation campaign. The location is also part of the recent EUREC4A campaign (Bony et al., 2017; Stevens et al., 2021).

DALES on its own, like several other atmospheric LEMs, has been evaluated under similar conditions—subtropical marine shallow cumulus convection. See for example, the LES model intercomparison studies for the non-precipitating BOMEX and ATEX cases (Siebesma et al., 2003; Stevens et al., 2001) and the precipitating RICO case (vanZanten et al., 2011).

Figure 3 shows the liquid water path and total water path in the GCM from the SP simulation mentioned above, compared to a corresponding simulation without SP, that is, using the standard OpenIFS. The SP columns show

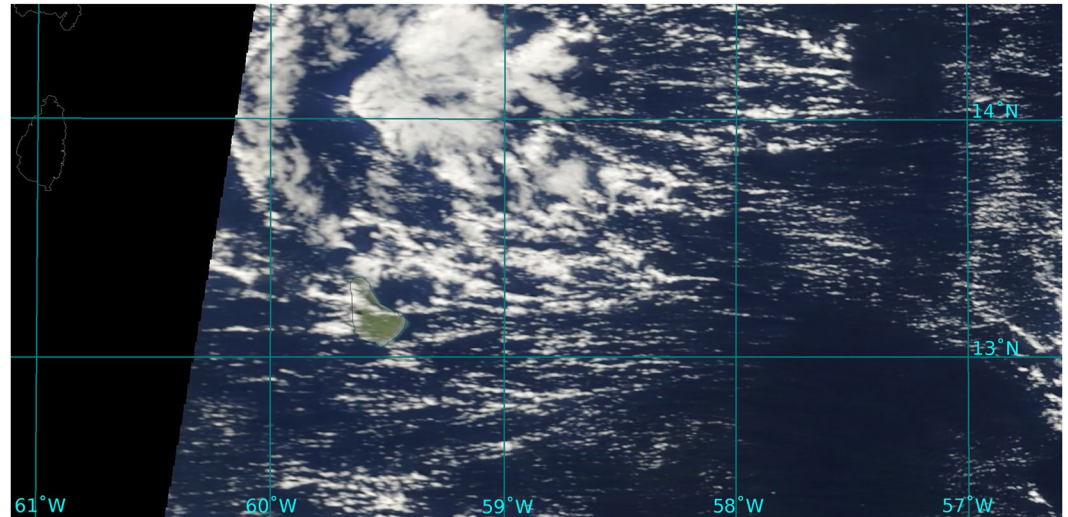


Figure 2. Satellite image from Terra/MODIS over the same region as Figure 1, on 2013-12-15 13:55 UTC.

virtually no clouds as opposed to the neighboring columns. The figure shows that the total water path in the two simulations are similar, while the liquid water path is markedly lower in the SP columns.

We will argue that the reason for the lack of clouds in the SP columns is because advection of clouds into the SP columns is suppressed by the SP coupling.

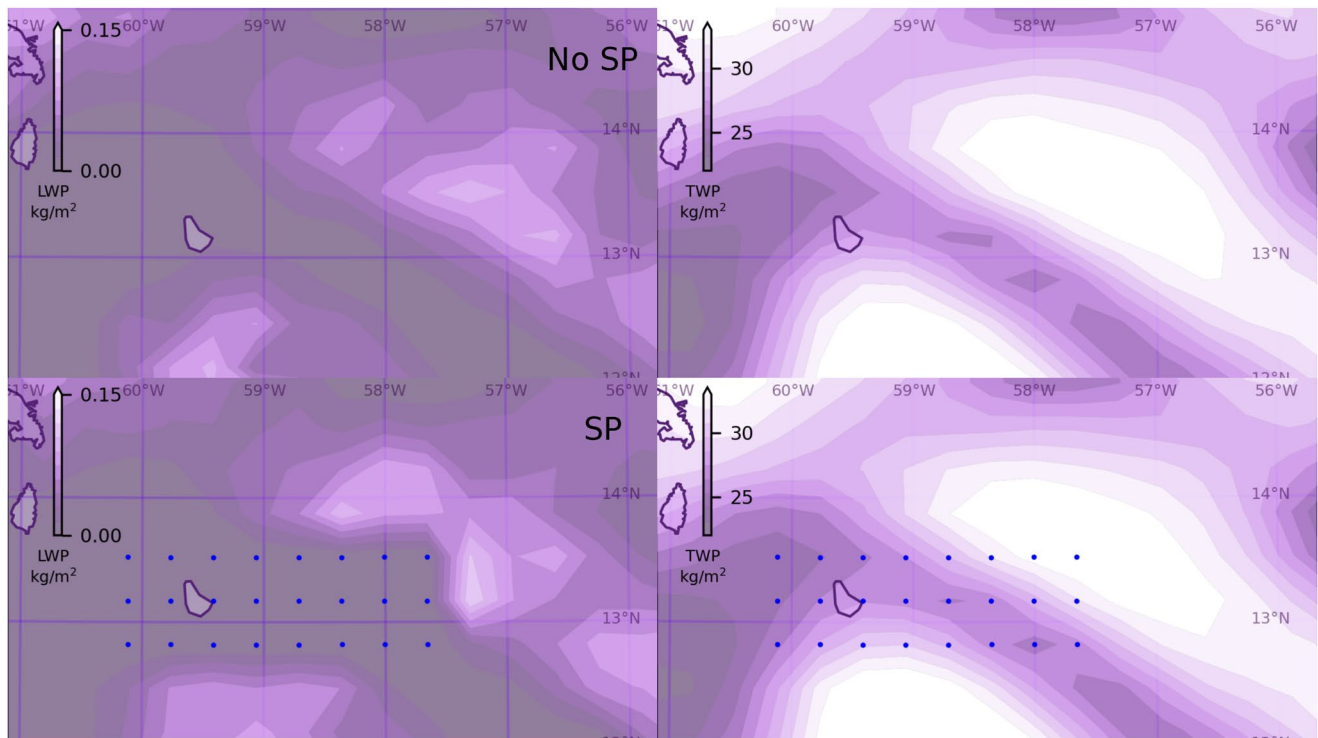


Figure 3. Comparing dynamics of the liquid water path and total water path in standard OpenIFS (top) and an superparameterization setup (bottom), in a simulation over Barbados. Superparameterized grid columns are marked with blue dots. The wind is from the east, advecting clouds in to the superparameterized regions. In the normal superparameterization, there is a hole in the cloud cover (seen in the liquid water path [LWP], left) over the superparameterized region, compared to standard OpenIFS. The total water path (TWP, right) is similar between the two simulations, and does not show different behavior in the superparameterized columns. The simulation was initialized on 2013-12-15 at 00 UTC, the image shows the state at 09:30.

This cloud suppression issue is especially visible in a regional SP model where the global model contains both superparameterized and regular columns next to each other as illustrated in Figure 3. The problem is not, however, restricted to regional SPs but can be expected also in uniformly superparameterized models.

2.2. Model Coupling in Superparameterization

For the physical model coupling between a LEM or another local model and some or all columns of a GCM, we have followed the same approach as described by Grabowski (2004). Since this coupling plays a crucial role in the cloud suppression, we briefly review the procedure here.

The general idea is that for each coupled variable, a forcing is introduced, which keeps the states of the two models consistent with each other,

$$\Phi(X, Y, Z, t) = \langle \phi(x, y, z, t) \rangle. \quad (1)$$

The brackets $\langle \cdot \rangle$ here denote a spatial average over the LEM domain in the horizontal directions. Capital letters denote variables in the GCM, small letters denote variables used in the LEM. Φ and ϕ here may represent any of the prognostic variables. The details of the regional SP setup used here are given in Jansson et al. (2019); we here give the coupling equations for reference.

The GCM first performs a single time step from time T to $T + \Delta T$, after which the LEM is evolved over the same time interval, in multiple smaller time steps of length Δt . Before the time evolution of each model, forcings are calculated based on the difference between the most recently obtained states of the two models, chosen such as to keep Equation 1 satisfied. The coupling and the time stepping of the system are described in the following four steps.

1. Given the state of both models at time T , represented by $\Phi(T)$ for any of the GCM variables and $\phi(T)$ for the corresponding LEM variable, the forcing F_ϕ on the variable Φ in the GCM is calculated as

$$F_\phi(T) = \frac{\langle \phi(T) \rangle - \Phi(T)}{\Delta T}. \quad (2)$$

2. Time-step the GCM

$$\Phi(T + \Delta T) = \Phi(T) + \Delta T [A_\phi(T) + S_\phi(T) + F_\phi(T)], \quad (3)$$

where $A_\phi(T)$ represents advection terms and $S_\phi(T)$ represents source terms for the variable Φ during the step from T to $T + \Delta T$.

3. Now the forcing on ϕ in the LEM is calculated as

$$f_\phi(T) = \frac{\Phi(T + \Delta T) - \langle \phi(T) \rangle}{\Delta T}. \quad (4)$$

4. and finally the time-step of the LEM is executed as

$$\phi(T + \Delta T) = \phi(T) + \sum_{t=T}^{T+\Delta T} \Delta t (a_\phi(t) + s_\phi(t) + f_\phi(T)). \quad (5)$$

The sums over t here represent evolving the LEM over several time steps, with $a_\phi(t)$ denoting advection terms and $s_\phi(t)$ denoting source terms for ϕ .

2.3. Coupling of DALES and OpenIFS

The SP of OpenIFS with DALES is formulated with couplings of variables for the horizontal wind velocities, temperature, and humidity. A summary the coupling is provided in Table 1. While OpenIFS uses the regular temperature T as a variable, DALES is formulated using the liquid water potential temperature θ_l ,

$$\theta_l \approx \frac{T}{\Pi(p)} - \frac{L}{c_{pd}\Pi(p)} q_c. \quad (6)$$

Table 1
Summary of the Coupling of OpenIFS and Dutch Atmospheric Large Eddy Simulation (DALES)

Coupled variables			
OpenIFS	Direction	DALES	Description
U, V	↔	u, v	Horizontal velocity
T	↔	θ_l	Temperature/liquid water potential temperature
$Q_V + Q_L + Q_I$	→	q_t	Specific total humidity
Q_V	←	$q_t - q_c$	Specific water vapor humidity
Q_L, Q_I	←	q_c	Specific condensed water humidity
A	←	a	Cloud fraction

Note. U and V are horizontal velocities, T is the temperature in OpenIFS, and θ_l is the liquid water potential temperature in DALES. Q_V , Q_L and Q_I are the specific water vapor, cloud liquid, and cloud ice amounts in OpenIFS, while q_t and q_c are the specific total water and cloud condensate amounts in DALES. The cloud fraction A is coupled only from DALES to OpenIFS.

where q_c is the specific cloud condensed water content and $c_{pd} \approx 1,004$ J/kg K is the specific heat of dry air at constant pressure. The Exner function $\Pi(p)$ is defined as

$$\Pi(p) = \left(\frac{p}{p_0} \right)^{R_d/c_{pd}}, \quad (7)$$

where $L \approx 2.5 \cdot 10^6$ J/kg is the latent heat of water vaporization, and $R_d \approx 287.04$ J/kg K is the gas constant for dry air.

2.4. Representation of Clouds and Small-Scale Variability

In this section, we will show how the different representations of clouds in the GCM and the LEM lead to an insufficient coupling of cloud quantities in SP and reduced advection of existing clouds into SP columns.

While the SP coupling described above conserves the amount of water in the system, it does not conserve the amount of condensed water. In global atmospheric models, the horizontal extent of a grid column is typically tens of kilometers, large enough to host numerous clouds. GCMs keep track of the amount of water vapor Q_V , liquid water Q_L , and ice water Q_I in each grid cell, along with the cloud-fraction A indicating that only a fraction of the grid cell is cloudy while the rest remains unsaturated.

LEM on the other hand, generally assume that the grid cells are either uniformly cloudy or unsaturated. Therefore cloud condensation only occurs if the grid cell is supersaturated by an all-or-nothing procedure. This allows the use of total specific humidity q_t , that is, the sum of condensed water and water vapor, as a prognostic variable from which the condensed water is only determined diagnostically. Virtually all atmospheric LEMs (e.g., SAM [Khairoutdinov et al., 2005], DALES [Heus et al., 2010], PALM [Maronga et al., 2015], MicroHH [van Heerwaarden et al., 2017], NICAM and SCALE [Tomita, 2008], and UCLALES [Stevens et al., 2005]) use q_t as a prognostic variable.

In SP schemes, the q_t variable of the LEM is forced toward the total specific humidity of the global model, see Table 1. If q_t increases above its saturation value, clouds will form in the LEM. However, GCM grid cells containing both clouds and unsaturated air are usually unsaturated on average, and as a result the LEM will be forced toward a cloud-free state, even though the GCM column contains clouds.

It is difficult to couple the amount of cloud condensed water in the same way as the other coupled quantities in a SP setup, as it is not a prognostic variable in the LEM but diagnosed from the local total specific humidity for each cell and time step. The amount of clouds in the LEM thus depends on fluctuations in state variables in the horizontal direction, which is a degree of freedom that so far is left uncoupled in SP schemes. In other words, the information contained in the GCM variables Q_L and Q_I is not transferred to the LEM in a standard SP scheme, since the LEM does not have corresponding prognostic variables to couple with these quantities.

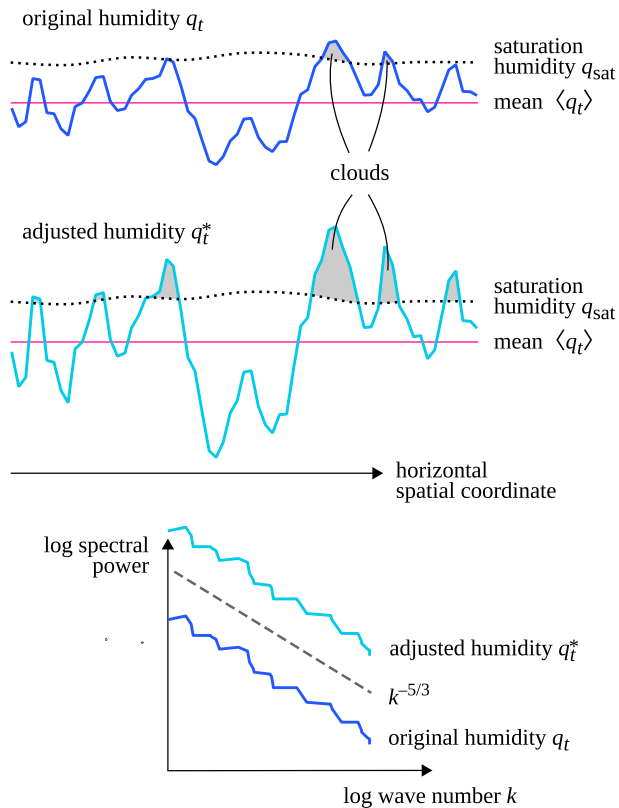


Figure 4. Illustration of the variability coupling procedure. Cells where q_t is above q_{sat} are saturated, and contribute to the condensed water content. The condensed water amount in each horizontal slab is controlled by adjusting the amplitude of the q_t fluctuations around the mean $\langle q_t \rangle$. This procedure preserves the shape (typically a $-5/3$ slope) of the humidity power spectrum.

Since clouds consist of local regions with higher humidity and/or lower temperature than their surroundings, we suggest that a way to control the cloudiness of the LEM is to nudge not just the horizontal average of the variables (as usually done in SP) but also the magnitude of their fluctuations from the average, in order to match the cloud-related variables of the large-scale model. This can be done in a way that leaves the fundamental relation (1) unchanged. A method to do so is described in Section 3.

Note that even without adjusting the horizontal fluctuations, the LEM can generate clouds through convection if the conditions are favorable. The difficulties described above appear only when existing clouds in the global model should be advected into a model column with an embedded LEM, which happens to be cloud-free.

3. Variability Coupling Procedure

To couple the cloud water content of the LEM with the global model, we propose an extension to the SP coupling scheme to influence not just the horizontal averages but also the horizontal variability. In particular, by changing the amplitude of the fluctuations of the total specific humidity in each horizontal grid plane, the condensed water amounts there will be influenced. We here consider clouds where the condensate consists of water only. If the fluctuations are adjusted without altering the horizontal average, this scheme is still compatible with the SP procedure. In other words, our proposed humidity variability coupling scheme amounts to re-distributing the total water content of each horizontal layer in the LEM, in such a way that the condensed water content matches the value from the GCM for each layer.

This adjustment scheme is in the spirit of the traditional SP formulation, where the two models are forced toward each other during each time step. Our scheme extends this idea to the condensed water content, which the traditional scheme doesn't couple from the GCM to the LEM. Coupling cloud condensate information in the other direction, from the LEM to the GCM, is

easily handled: the forcing on the GCM can be derived from the diagnosed specific condensed water humidity q_c of the LEM.

3.1. Humidity Variability

There are many ways to adjust the total humidity field—any perturbation which leaves the horizontal average unchanged, and does not introduce negative humidity values could be considered. We choose to scale the amplitude of existing variations in each horizontal layer. In this way, we do not have to specify the length scales of the variability we add, but merely amplify the existing variability, as illustrated in Figure 4. Let q_t be the total humidity and q_{sat} the saturation humidity for each cell in the LEM.

The condensed water humidity is then

$$q_c = \max [0, q_t - q_{\text{sat}}(p, T)]. \quad (8)$$

The modified q_t field can be written as

$$q_t^* = \beta (q_t - \langle q_t \rangle) + \langle q_t \rangle \quad (9)$$

where β is a scaling factor, chosen separately for each horizontal layer. If $\beta = 0$ all variations of q_t around its mean are removed, if $\beta < 1$ the variability of q_t is decreased, if $\beta = 1$ q_t is left unchanged, and for $\beta > 1$ the variability is amplified. This scaling leaves the average of q_t unchanged. A consequence of this manner of adjusting the variability is that the spatial Fourier spectrum of the q_t -field retains its shape, only the amplitude is changed. Another choice we make here is to keep the temperature T in each grid cell unchanged while adjusting q_t , which

requires adjusting the liquid water potential temperature θ_l . This choice, which is further discussed below, has an important consequence for the coupling procedure, namely that the saturation humidity q_{sat} in each grid cell, which depends on temperature and pressure, remains unchanged during the adjustment.

Next we determine β so that the average condensed water humidity q_c in the horizontal layer matches the condensed water humidity $Q_C = Q_L + Q_I$ of the GCM,

$$Q_C = \langle q_c(\beta) \rangle = \langle \max(0, q_l^*(\beta) - q_{\text{sat}}) \rangle. \quad (10)$$

Combining Equations 9 and 10 gives

$$Q_C = \langle \max[0, \beta q_l + (1 - \beta)\langle q_l \rangle - q_{\text{sat}}] \rangle. \quad (11)$$

The max operator makes this equation difficult to handle analytically, so we solve it numerically for each horizontal layer. If $Q_C > \langle q_l \rangle$, we obtain a $\beta > 1$ and the LES q_l variability and the cloud amount is increased, if $Q_C < \langle q_l \rangle$, $\beta < 1$ and the LES cloud amount is decreased.

3.2. Maintaining a Constant Temperature While Coupling Humidity

In determining the variability scaling β above, it was assumed that q_{sat} remains unchanged as β is varied. Since q_{sat} is a function of temperature and pressure, this assumption holds if the temperature remains constant as β is varied, as pressure is assumed to be a function only of height. In order to keep the temperature T constant while adjusting q_c , θ_l has to be adjusted as well.

$$\Delta\theta_l = -\frac{L}{c_{pd}\Pi(p)}\Delta q_c, \quad (12)$$

where Δq_c is the change in cloud condensate caused by the change in q_l .

Also for physical reasons it is preferable to adjust the humidity while keeping the temperature constant. In cloud parameterization schemes, it is generally assumed that variability in humidity is decisive for cloud formation, while variability in temperature plays a minor role (Price & Wood, 2002). When adjusting the variability of the humidity, we change the condensed water content of the local model. There is no latent heat or temperature change associated with this re-distribution, in the same way as advection of clouds from one grid cell to another leaves the temperature unaffected.

If one makes a different choice here, to for example keep θ_l constant during the adjustment, the following issues should be noted. The temperature-dependence of q_{sat} must be considered while solving Equation 11. Otherwise the adjustment scheme will add less clouds than intended, because q_l increases with the addition of cloud condensate. Allowing T to change in the adjustment affects the buoyancy of the newly added clouds, which may in turn affect their lifetime. Adjusting variability at constant T adds less buoyancy to the new clouds than adjusting at constant θ_l .

3.3. Implementation Details

While the coupling tendencies on the local models in an SP setup are generally applied gradually over time, we have implemented the variability changes instantly at every time step of the large-scale model. One reason for this is that the small-scale fields move due to advection over the course of one large-scale time step, which means that the tendencies need to move as well in order to achieve the desired final structure. Also with an instant adjustment, it is easier to verify that the procedure actually achieves the correct cloud condensate amounts.

Some practical issues in the adjustment procedure need to be handled:

1. Equation 11 for β may give an unreasonably large β as the solution. As this can make the local model unstable, we restrict β to the range 0...5. The permissible range of β is typically exceeded when large-scale advection would add clouds above the boundary layer, where the local model has a small variability in the horizontal direction. In this case, we add white noise to q_l , again with the amplitude selected to give the desired amount of cloud condensate.

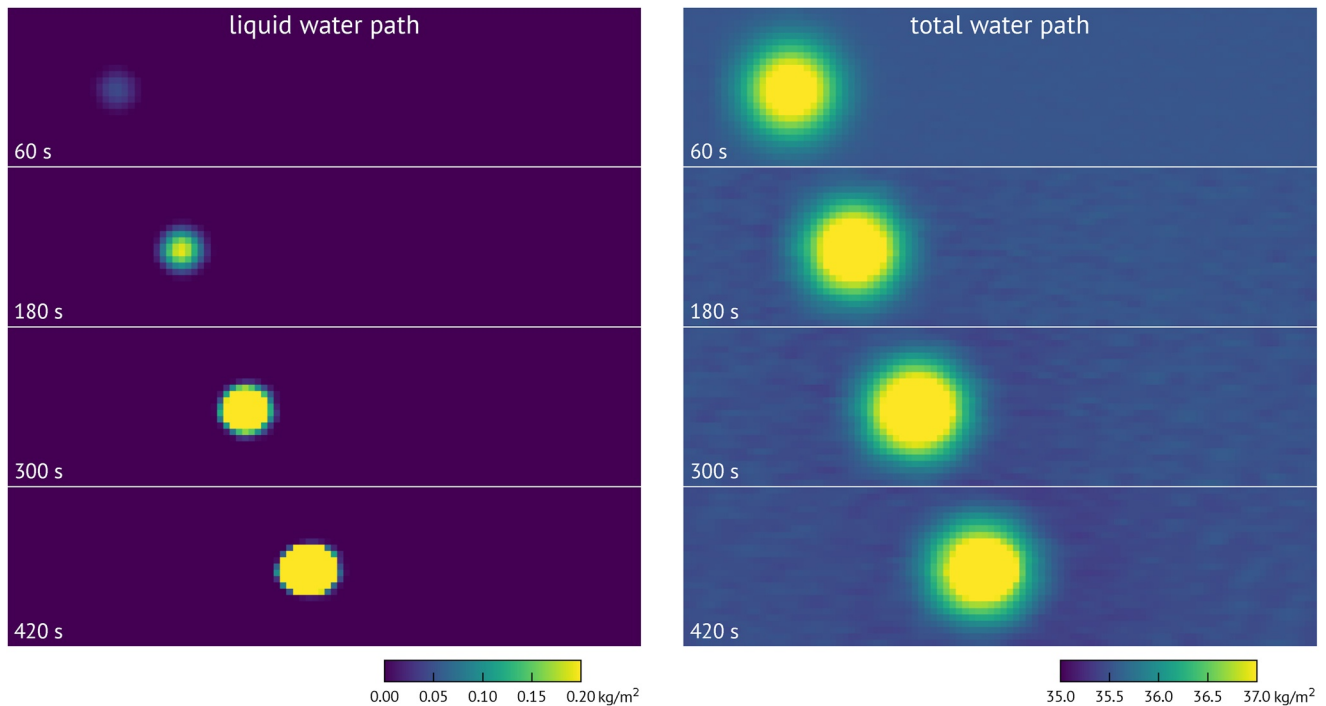


Figure 5. A moist-bubble experiment with a single large eddy simulation domain. The plots show the liquid water path and total water path.

2. q_t is not allowed to become negative in the adjustment. We have found that when limiting β as above, the procedure does not cause negative q_t values. As a precaution, one can set negative q_t values to 0, and adjust the other cells in the same horizontal layer to conserve the total mass of water.
3. If $Q_c = 0$, β is not uniquely determined. If q_c is also 0, we set $\beta = 1$, implying no variability adjustment. If $q_c > 0$ we nudge the layer toward just below saturation that is, $\beta < 1$ but as large as possible.
4. With OpenIFS as the global model, sometimes Q_c is positive but tiny, on the order of 10^{-12} kg/kg. We choose to ignore condensed water humidities $< 10^{-9}$ kg/kg, when they would result in a nudge toward more variability.

The choices in (3) and (4) seem less critical than the rest in our experience, our motivation is to make the smallest possible intervention in the case where the size of the required variability adjustment is not uniquely defined.

4. Advection and Variability Coupling in a Simplified SP Setup

To illustrate the problems with cloud advection in SP as well as the solutions and limitations provided by the proposed humidity variability coupling scheme, we show a simplified SP setup where the large-scale model consists of only (upwind) advection of the prognostic variables, with a fixed large-scale wind. We construct this model as a realization of the following thought experiment: consider an SP simulation where a single LEM contains a cloud but has an average humidity below saturation, and ask if or how this cloud can be advected into an LEM at a neighboring grid point. This model provides a simple setting to illustrate the cloud advection problem in SP and to see how the variability coupling approach mitigates the problem.

The ideal behavior in this experiment is shown in Figure 5 with a single wide LEM. A superparameterized version is shown in Figure 6, with four LEMs placed side by side. The LEMs are initialized with vertical profiles from the BOMEX case included with the DALES model. The left-most LEM is perturbed with a bubble of moist air, chosen to develop into a single cloud. There is a uniform wind to the right, advecting the cloud. The figure shows snapshots of the liquid water path and total water path in both simulations. In this experiment, the wind is 10 m/s to the east, the DALES domains are 2.5×2.5 km in the horizontal direction with a 100 m resolution, and 5 km high with a 40 m resolution in the vertical. The initial bubble perturbation of q_t in the left-most LEM has

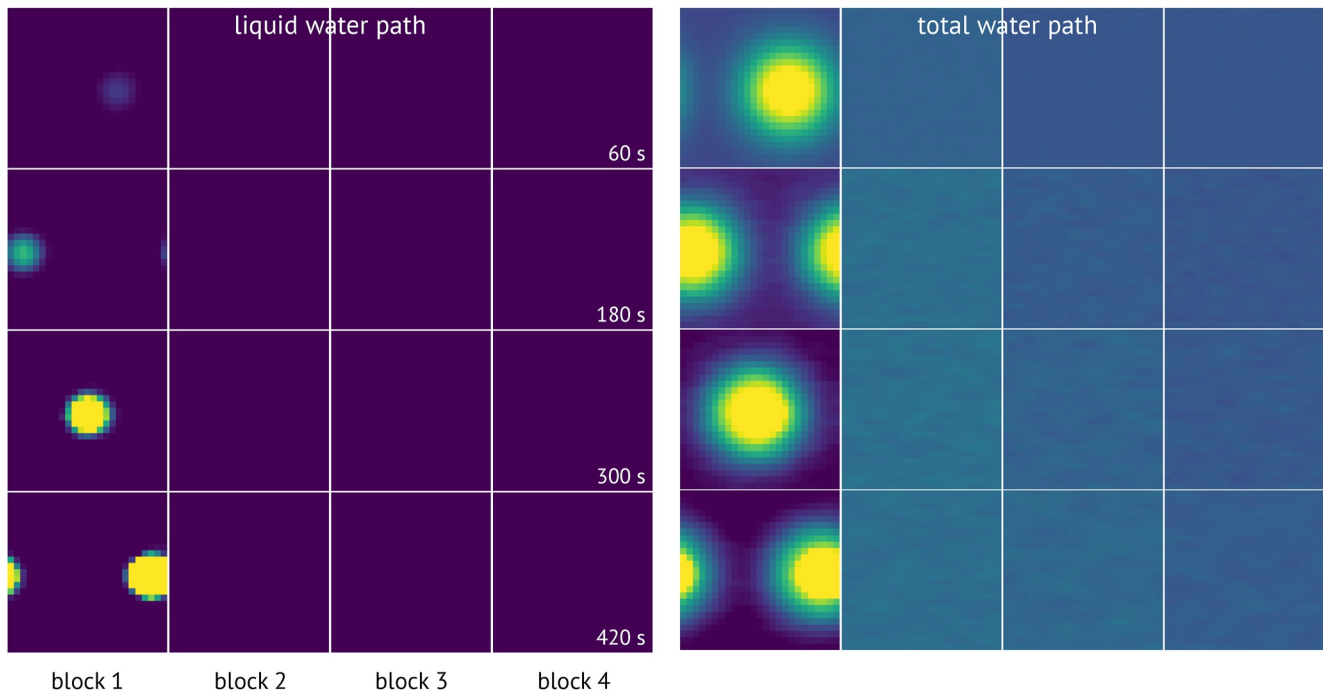


Figure 6. A superparameterized moist-bubble experiment with four small-scale domains and where the large-scale model consists of advection only.

a Gaussian shape with standard deviation of 500 m and a central amplitude of 1.5 g/kg, with the center at 800 m above the ground.

The experiment shows that with SP, the cloud stays in the left-most LEM where it was created, cycling around the periodic boundary conditions of the domain. The large-scale advection of total humidity and temperature is not sufficient to transfer any cloud condensate to the neighboring LEM. This experiment shows that even though temperature and the total humidity q_t is advected correctly according to the idea of SP, this is not always sufficient for clouds (as measured with cloud cover or cloud condensed water content) to be advected—in particular when the clouds are on the sub-grid-scale of the large-scale model.

Figure 7 shows the simplified SP setup with the same moist bubble perturbation as in Figure 6. With the variability coupling scheme, we can see that clouds are advected between the LEMs. The increased variability in the total water content from the variability coupling procedure can be seen in the total water path on the right. An animation of the three simulations with this simplified SP setup is available as Movie S1.

Even with the variability coupling, the bubble experiment is a particularly difficult case for SP: the cloud in the leftmost LEM forms a single coherent structure, which is absent in the other LEMs. Figure 7 shows that the shape of the clouds is not preserved when they move between the LEMs—this would require an even more detailed coupling of the LEMs.

Experiments with the simplified SP model shows that the clouds added with variability adjustment tend to dissipate over time—even though the adjustment initially generates the desired amount of $\langle q_c \rangle$, the local models may not retain the imposed amounts of clouds when evolved in time, showing that the cloud condensate amount is a difficult property to control. This can be seen as fluctuations in the cloud condensate amount in Figure 8 and also in Movie S1.

5. Results of Superparameterized Barbados Simulation With Variability Coupling

To see the full effects of the variability coupling procedure introduced above, we repeat the Barbados simulation from Section 2 with the variability coupling scheme (9) enabled.

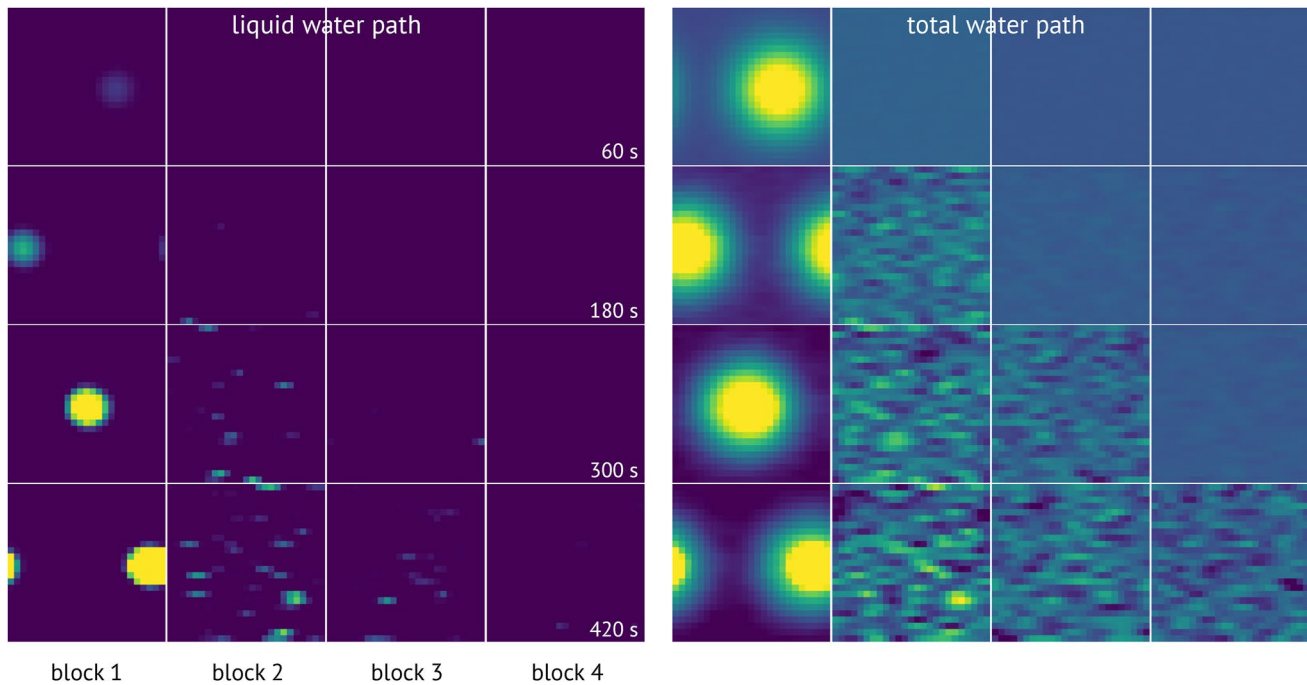


Figure 7. The moist-bubble experiment with four coupled local models shown in Figure 6 repeated with variability coupling.

Figure 9 show the Barbados simulation repeated with the variability coupling scheme. The LEMs clearly contain more clouds compared to the standard SP coupling scheme (Figure 1), and clouds can be advected into the SP region to a significantly higher degree than with the standard scheme. An animation comparing the three simulations shown in Figures 1, 3 and 9 is available as Movie S2.

A quantitative comparison of the clouds in the three different Barbados simulations is given in Figure 10, which shows east-west profiles of the liquid water path and low cloud cover. The data has been averaged over time, 04–12 hr UTC, and over the north-south extent of the SP domain that is, three rows of GCM grid points. Comparing the experiments shows that SP causes a marked drop in clouds in the SP domain, both in liquid water path and in cloud cover, compared to the non-SP simulation.

The variability coupling method increases the cloud content compared to standard SP, but is not sufficient to reach the levels of the non-SP simulation.

One reason we still see a lack of cloud condensate with the variability coupling, is that the clouds added by variability adjustment dissipate too quickly, as in the simplified SP experiment. The dissipation of the clouds can be seen in Figure 11, showing vertical profiles of the cloud condensate q_l over time for two neighboring columns at the eastern border of the SP domain. Panel (a) shows the OpenIFS Q_L for a non-SP column, and panels (b and c) show the neighbor SP column downwind (easternmost column in the middle row of the SP domain). Panel (b) shows the case of variability coupling, while panel (c) is without variability coupling. The same phenomenon can be seen in the Movies S1 and S2, where the cloud fields get noticeably brighter at the coupling time steps and then fade away again.

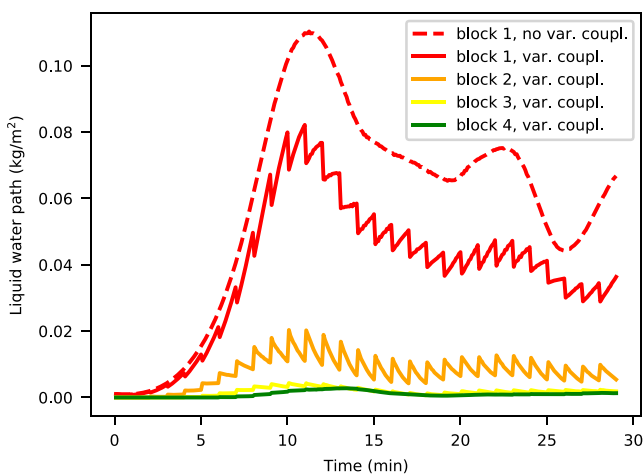


Figure 8. Time development of the horizontally averaged liquid water path in the moist bubble experiment. The dashed curve shows the first (leftmost) Large Eddy Simulation (LES) of the simulation without variability coupling (Figure 6). The solid lines show the LES domains in the simulation with variability coupling (Figure 7). The saw-tooth waveform has the same period as the superparameterization coupling time steps, the sharp edges coincide with the coupling time steps.

6. Discussion and Conclusions

We have used DALES as a SP in the IFS for a region over the subtropical Atlantic Ocean that is dominated by shallow cumulus convection. When DALES is coupled in the traditional way, as described in Sections 2.2 and

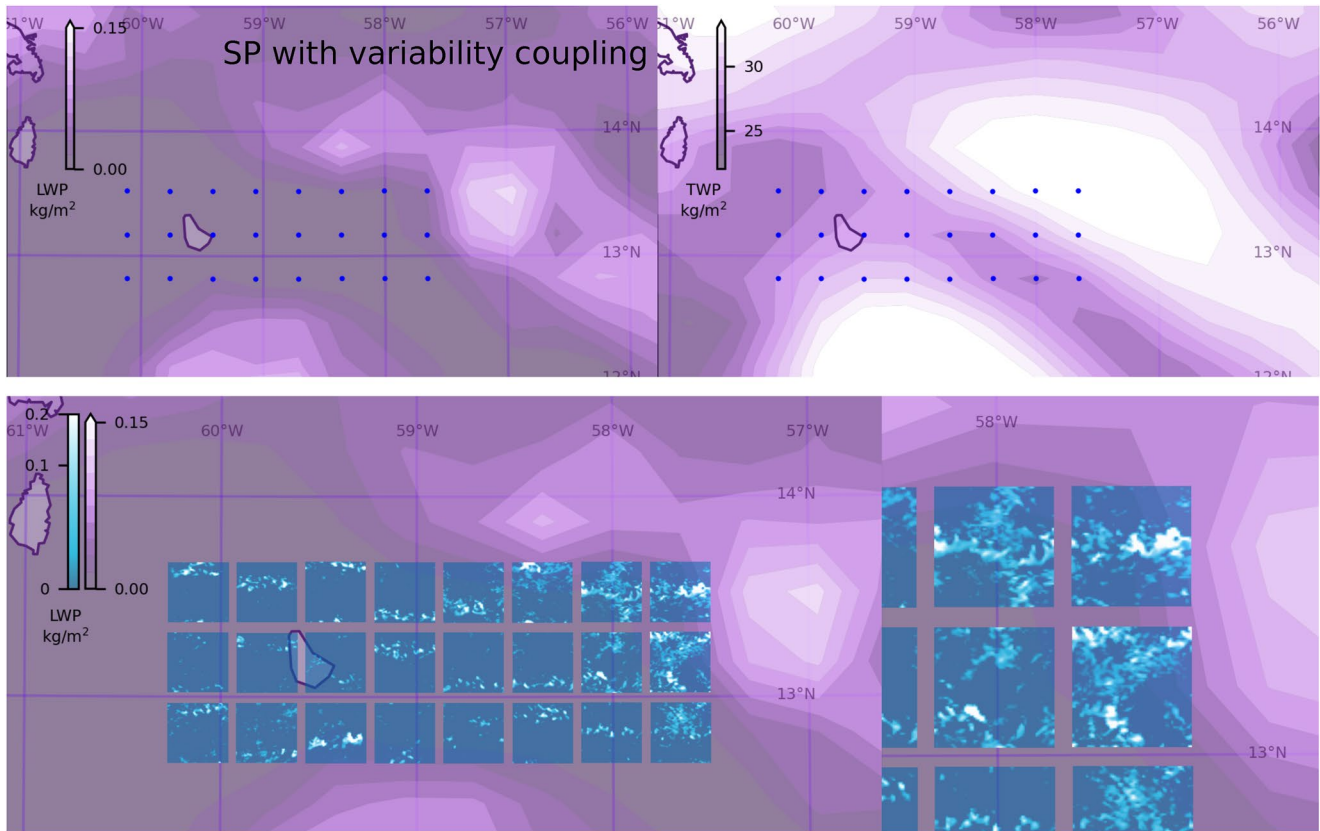


Figure 9. Superparameterization with variability coupling, in a simulation over Barbados on 2013-12-15.

2.3, the cloud amount in the superparameterized region is strongly underestimated both in cloud cover as well as in liquid water content. One possible cause for this underestimation of cloud amount that has been hypothesized in this study is the use of moist conserved prognostic variables by DALES, such as the total specific humidity q_t , rather than the liquid water and the water vapor separately. As a result any changes of the cloud liquid water in the IFS, for instance by advection, has to be passed on to DALES via q_t . In practice this means that the liquid water from the IFS is distributed uniformly as an increment of q_t for all gridpoints in the LEM. Since the LEM is usually only partially cloudy this effectively implies that most of the liquid water from the IFS is added as water vapor to the LEM unsaturated gridpoints. To illustrate this problem we have analyzed in Section 4 an evolving single cloudy updraft that is advected from West to East in an unsaturated environment. When superparameterizing this case, it is easy to observe and understand that the liquid water advected out of the cloud-containing LEM to its neighboring LEM ends up as water vapor in the neighboring LEM. We then anticipated that this problem also shows up in any other superparameterized model system that use CRMs with moist conserved variables such as for instance SAM (Khairoutdinov et al., 2005).

In Section 3 we propose an alternative approach that allows the communication of the advected liquid water between the IFS to the LEM. In doing so it is important to realize that liquid water in a partially cloudy atmosphere is the result of spatial variability of the total water specific humidity, where the condensed water is merely the result of the positive fluctuations in the total water that exceed saturation. Therefore it is proposed to include the advected liquid water from the IFS into the LEM by increasing the variability of q_t accordingly. In doing so we have imposed two extra constraints: (a) the added moisture variability should not change the domain averaged total water specific humidity and (b) the added variability should not have a preferred length scale, that is, variability has to be added equally at all spatial length scales. A simple procedure that fulfills all these conditions is given by Equation 9 where the scaling factor β has to be chosen such that the increased moisture variability precisely provides the desired liquid water change as dictated by the IFS.

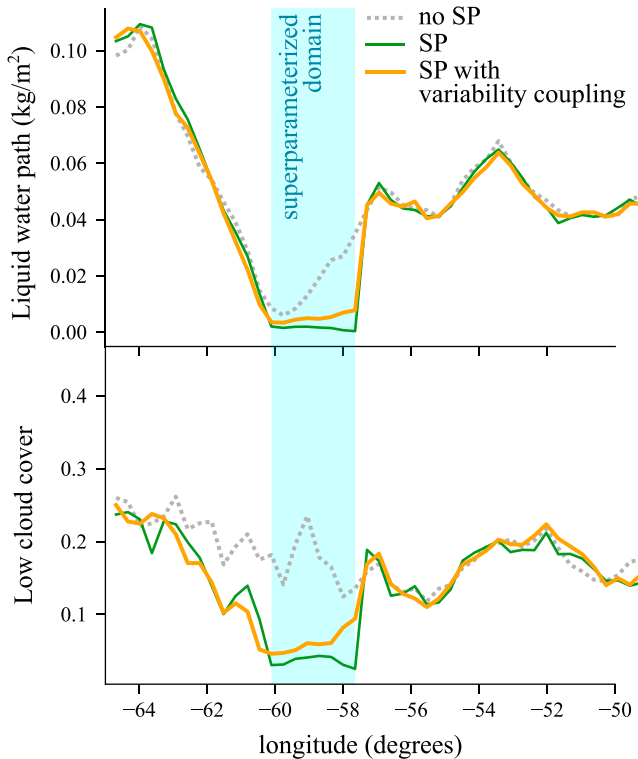


Figure 10. East-west profiles of low cloud cover and liquid water path for the three Barbados simulations: no SP, SP, and SP with variability coupling. The data is averaged over 8 hr (04–12 UTC) and over the north–south extent of the SP domain. The SP domain is indicated with a blue background. The low cloud cover measure is from OpenIFS and is defined as the cloud cover between the surface and the height of 80% of the surface pressure (roughly 2 km). SP = superparameterization.

Unfortunately the improvement due to this humidity variability coupling is only marginal, both for the Barbados experiment as well as for the idealized bubble experiment. In both cases the LEM diffuses the added variability away within the time step of the large-scale model. As a result, the more downstream LEMs receive ever smaller amounts of liquid water by advection which explains why the improvement of proposed modification deteriorates strongly in the more downstream LEMs.

So why does the humidity variability coupling give such a marginal improvement? And is it not possible to avoid the need for introducing the variability coupling in first place? One might be tempted to answer the last question positively by using a LEM that employs liquid water and ice as prognostic variables and couple these to the IFS in the same manner as the other prognostic quantities. However, in that case the advected liquid water into the local LEM will be uniformly distributed over the horizontal grid of the LEM. As a result all the advected liquid water in the unsaturated grid points will evaporate almost instantaneously. So also in the case of using a LEM with prognostic cloud condensate, dedicated choices need to be made how to spatially distribute the advected liquid water into the local LEM. The Goddard multiscale modeling framework (Chern et al., 2016, 2020; Tao et al., 2009) for instance, is using a LEM with prognostic cloud condensate. In their framework the large scale advected cloud condensate is only added to saturated grid points of the LEM and proportionally to the already existing cloud amount in each grid point, very similar to the humidity variance coupling proposed in this study. So the use of prognostic cloud condensate in the local LEM requires similar redistribution choices as in the present case where we use a LEM with moist conserved variables.

This leaves us with the question why the SP so strongly underestimates the cloud condensate, even when the humidity variability coupling is in place. We can think of at least two reasons. First, it is well possible the parameterized convection outside the SP region results in mean thermodynamic profiles that are too stable for a local LEM to generate moist convection and clouds. Although the local LEMs are only active inside the SP region where

convection parameterization is switched off, we verified that the SP grid cells directly neighboring the upstream parameterized grid cells have very similar vertical thermodynamic structures as their parameterized grid point neighbors. So it is well possible that these thermodynamic structures support parameterized clouds but not necessarily resolved clouds. In that case the added liquid water in the SP grid cells will be largely evaporated by the local thermodynamics of the LEM within the IFS timestep. A second reason is related to the (in)capability of the LEMs to represent the observed cloud structures (see Figure 2) that have spatial scales well beyond the domain size of the local LEMs. These large mesoscale cloud structures are the rule rather than the exception (Stevens et al., 2020). The employment of a local LEM with periodic boundary conditions and a rather small domain size of only 12.8 km will only show up as spatially unorganized sample of saturated updrafts with possibly a resulting cloud fraction much lower than the actual observed mesoscale cloud structure. Organized cloud structures in this region associated with cold pools, aka “gravel,” have been shown be the most abundant type of organization (Bony et al., 2020) but are only faithfully simulated by LEMs with domains larger than 25 km (Seifert & Heus, 2013). Furthermore shallow cumulus convection such as observed during ATEX where the clouds are topped by spreading anvils below a sharp inversion are difficult to simulate consistently by LEMs and depend strongly on the used vertical resolution (Stevens et al., 2001). These outflow structures for which now the name “flowers” has been coined (Stevens et al., 2020) are frequently observed over the subtropical Atlantic Ocean.

Likely, both proposed mechanisms are responsible for the observed cloud dissipation. One way to find out which is the most dominant process is to conduct a very large eddy simulation over a domain at least as large as the SP region indicated in Figure 1 as a benchmark using periodic boundary conditions. Repeating the simulation by dividing it up as a collection of smaller LEMs coupled in the same spirit as the bubble experiment and comparing

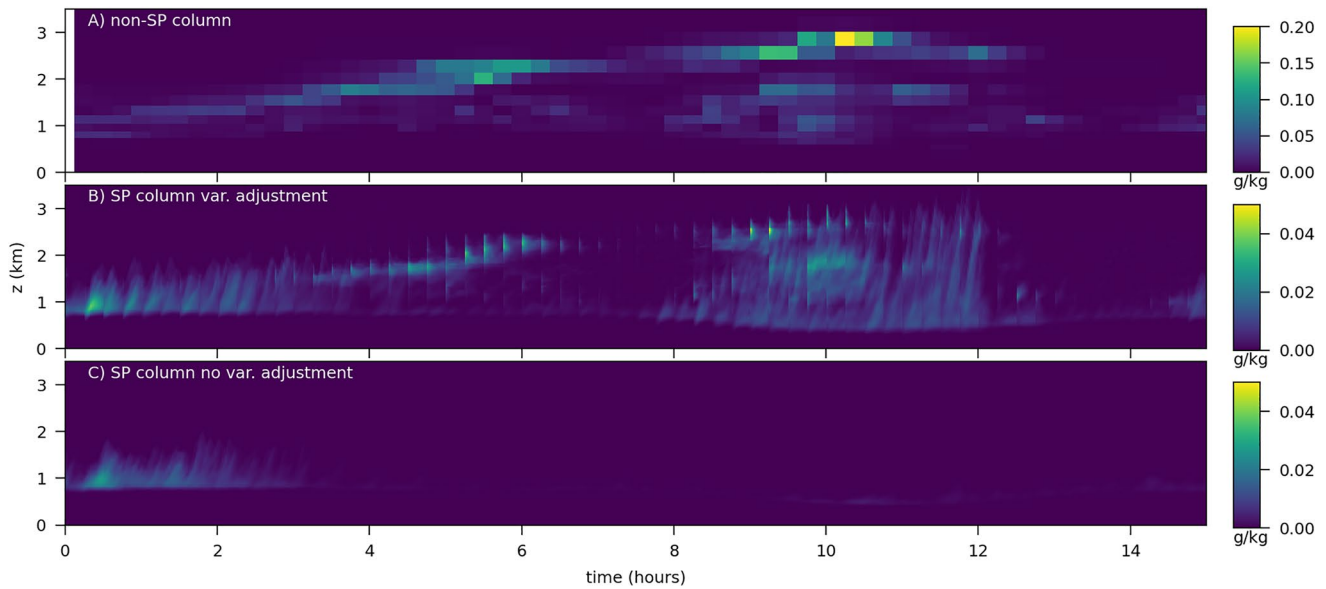


Figure 11. Vertical profiles of cloud liquid water in the superparameterized simulations. (a) The non-superparameterized column just upwind (to the east) of the middle row of the superparameterization (SP) domain. (b) The middle row, easternmost Large Eddy Simulation (LES) of the SP domain, with variability coupling. (c) The same LES, without variability coupling. In panel (b), the time steps of the GCM, 15 min apart, show up as sharp features due to the variability adjustment of the total humidity. Note that panel (a) has a different color scale with higher cloud condensate amounts.

the results of the large domain simulation and the SP-version over the same domain should allow to reveal the error in the cloud amount of the small LEMs due to their incapability of representing the mesoscale organization. Such a Big Brother experiment might also be instructive for testing the realism of exascale high resolution SP enterprises on GPUs (Hannah et al., 2020).

Finally, one may also wonder whether the negative cloud bias in the SP region would also show up in “stand-alone” Large Eddy Simulations that are forced with dynamical advective tendencies from a large-scale model rather than with the nudging procedure explained in Section 2.2. The answer to this question is yes when it concerns errors and biases related to domain size and resolution. It is more difficult to answer whether driving the LEM with large scale tendencies would be more accurate than forcing it with the nudging process. Using large scale tendencies rather than nudging to thermodynamics profiles with too short timescales has the advantage that one avoids the risk of imposing profiles that are never in quasi-equilibrium with the smaller scale turbulence state. The risk of imposing only advective large scale tendencies on the other hand is that LEM might give a more realistic response but related to a large scale state that has drifted away from the desired large scale state.

Data Availability Statement

Dutch Atmospheric Large Eddy Simulation (DALES), OMUSE, the superparameterization (SP) coupler for DALES and OpenIFS, and the Simple SP experiment are available on GitHub under open-source licenses. DALES: (Arabas et al., 2021), <https://github.com/dalessteam/dales>, <https://doi.org/10.5281/zenodo.3759192>. OMUSE: (Pelupessy et al., 2021), <https://github.com/omuse-geoscience/omuse>, <https://doi.org/10.5281/zenodo.3755558>. SP coupler: (Jansson et al., 2018), <https://github.com/CloudResolvingClimateModeling/sp-coupler>, <https://doi.org/10.5281/zenodo.1968304>. Version 1.1 which was used in this work contains the variability coupling. Version 1.0 was used in our previous study (Jansson et al., 2019). The simple SP experiment: (Jansson et al., 2021), <https://github.com/CloudResolvingClimateModeling/Simple-SP>, <https://doi.org/10.5281/zenodo.5511753>. For OpenIFS, a license can be requested from ECMWF. For details of the SP setup with OpenIFS with DALES, see also Jansson et al. (2019). The Python interface to DALES using OMUSE is described in van den Oord et al. (2020).

Acknowledgments

The authors thank Glenn Carver at the ECMWF for help with OpenIFS and for providing us with initial states for the simulation, and Jiun-Dar Chern who provided information on the Goddard MMF. The authors are grateful to Mike Pritchard and two anonymous reviewers for constructive comments on the manuscript. The authors acknowledge the use of imagery from the NASA Worldview application (<https://worldview.earthdata.nasa.gov/>) operated by the NASA/Goddard Space Flight Center Earth Science Data and Information System project. This work was supported by the Netherlands eScience Center under Grant No. 027.015.G03. Furthermore, the authors acknowledge the use of ECMWF's computing and archive facilities in the research reported here. Also SURFSara provided computing resources.

References

Arabas, S., Axelsen, S., Attema, J., Beets, C., Boeing, S. J., de Bruine, M., et al. (2021). DALES 4.3. <https://doi.org/10.5281/zenodo.4604726>

Arakawa, A., Jung, J.-H., & Wu, C.-M. (2011). Toward unification of the multiscale modeling of the atmosphere. *Atmospheric Chemistry and Physics*, *11*(8), 3731–3742. <https://doi.org/10.5194/acp-11-3731-2011>

Arakawa, A., Jung, J.-H., & Wu, C.-M. (2016). Multiscale modeling of the moist-convective atmosphere. *Meteorological Monographs*, *56*, 16.1–16.17. <https://doi.org/10.1175/AMSMONOGRAPHIS-D-15-0014.1>

Bony, S., & Dufresne, J.-L. (2005). Marine boundary layer clouds at the heart of tropical cloud feedback uncertainties in climate models. *Geophysical Research Letters*, *32*(20), L20806. <https://doi.org/10.1029/2005GL023851>

Bony, S., Schulz, H., Vial, J., & Stevens, B. (2020). Sugar, gravel, fish, and flowers: Dependence of mesoscale patterns of trade-wind clouds on environmental conditions. *Geophysical Research Letters*, *47*(7), e2019GL085988. <https://doi.org/10.1029/2019GL085988>

Bony, S., Stevens, B., Ament, F., Bigorre, S., Chazette, P., Crewell, S., et al. (2017). EUREC4A: A field campaign to elucidate the couplings between clouds, convection and circulation. *Surveys in Geophysics*, *38*(6), 1529–1568. <https://doi.org/10.1007/s10712-017-9428-0>

Chern, J.-D., Tao, W.-K., Lang, S. E., Li, X., & Matsui, T. (2020). Evaluating precipitation features and rainfall characteristics in a multi-scale modeling framework. *Journal of Advances in Modeling Earth Systems*, *12*(8), e2019MS002007. <https://doi.org/10.1029/2019MS002007>

Chern, J.-D., Tao, W.-K., Lang, S. E., Matsui, T., Li, J.-L. F., Mohr, K. I., et al. (2016). Performance of the Goddard multiscale modeling framework with Goddard ice microphysical schemes. *Journal of Advances in Modeling Earth Systems*, *8*(1), 66–95. <https://doi.org/10.1002/2015MS000469>

Grabowski, W. W. (2001). Coupling cloud processes with the large-scale dynamics using the cloud-resolving convection parameterization (CRCP). *Journal of the Atmospheric Sciences*, *58*(9), 978–997. [https://doi.org/10.1175/1520-0469\(2001\)058<0978:CCPWTL>2.0.CO;2](https://doi.org/10.1175/1520-0469(2001)058<0978:CCPWTL>2.0.CO;2)

Grabowski, W. W. (2004). An improved framework for superparameterization. *Journal of the Atmospheric Sciences*, *61*(15), 1940–1952. [https://doi.org/10.1175/1520-0469\(2004\)061<1940:AIFFS>2.0.CO;2](https://doi.org/10.1175/1520-0469(2004)061<1940:AIFFS>2.0.CO;2)

Grabowski, W. W. (2016). Towards global large eddy simulation: Super-parameterization revisited. *Journal of the Meteorological Society of Japan. Series II*, *94*(4), 327–344. <https://doi.org/10.2151/jmsj.2016-017>

Grabowski, W. W., & Smolarkiewicz, P. K. (1999). CRCP: A cloud resolving convection parameterization for modeling the tropical convecting atmosphere. *Physica D: Nonlinear Phenomena*, *133*(1), 171–178. [https://doi.org/10.1016/S0167-2789\(99\)00104-9](https://doi.org/10.1016/S0167-2789(99)00104-9)

Hannah, W. M., Jones, C. R., Hillman, B. R., Norman, M. R., Bader, D. C., Taylor, M. A., et al. (2020). Initial results from the super-parameterized E3SM. *Journal of Advances in Modeling Earth Systems*, *12*(1), e2019MS001863. <https://doi.org/10.1029/2019MS001863>

Heus, T., van Heerwaarden, C. C., Jonker, H. J. J., Pier Siebesma, A., Axelsen, S., van den Dries, K., et al. (2010). Formulation of the Dutch Atmospheric Large-Eddy Simulation (DALES) and overview of its applications. *Geoscientific Model Development*, *3*(2), 415–444. <https://doi.org/10.5194/gmd-3-415-2010>

Jansson, F., van den Oord, G., & Pelupessy, I. (2018). Superparameterization coupler library. Programming language: Python. <https://doi.org/10.5281/zenodo.1968305>

Jansson, F., van den Oord, G., Pelupessy, I., Chertova, M., Grönqvist, J. H., Siebesma, P., & Crommelin, D. (2021). simple-sp: V1.0. <https://doi.org/10.5281/zenodo.5511753>

Jansson, F., van den Oord, G., Pelupessy, I., Grönqvist, J. H., Siebesma, A. P., & Crommelin, D. (2019). Regional superparameterization in a global circulation model using large eddy simulations. *Journal of Advances in Modeling Earth Systems*, *11*(9), 2958–2979. <https://doi.org/10.1029/2018MS001600>

Khairoutdinov, M., Randall, D., & DeMott, C. (2005). Simulations of the atmospheric general circulation using a cloud-resolving model as a superparameterization of physical processes. *Journal of the Atmospheric Sciences*, *62*(7), 2136–2154. <https://doi.org/10.1175/JAS3453.1>

Lin, G., Jones, C. R., Leung, L. R., Feng, Z., & Ovchinnikov, M. (2022). Mesoscale convective systems in a superparameterized E3SM simulation at high resolution. *Journal of Advances in Modeling Earth Systems*, *14*(1), e2021MS002660. <https://doi.org/10.1029/2021MS002660>

Malardel, S., Wedi, N., Deconinck, W., Diamantakis, M., Kuehnlein, C., Mozdzyński, G., et al. (2016). *A new grid for the IFS* (pp. 23–28). ECMWF Newsletter. <https://doi.org/10.21957/zwd9u5i>

Maronga, B., Gryscha, M., Heinze, R., Hoffmann, F., Kanani-Sühring, F., Keck, M., et al. (2015). The parallelized large-eddy simulation model (PALM) version 4.0 for atmospheric and oceanic flows: Model formulation, recent developments, and future perspectives. *Geoscientific Model Development*, *8*(8), 2515–2551. <https://doi.org/10.5194/gmd-8-2515-2015>

Parishani, H., Pritchard, M. S., Bretherton, C. S., Wyant, M. C., & Khairoutdinov, M. (2017). Toward low-cloud-permitting cloud superparameterization with explicit boundary layer turbulence. *Journal of Advances in Modeling Earth Systems*, *9*(3), 1542–1571. <https://doi.org/10.1002/2017MS000968>

Pelupessy, I., van den Oord, G., Jansson, F., Verstraaten, M., van Werkhoven, B., Baars, S., et al. (2021). OMUSE. <https://doi.org/10.5281/zenodo.5006102>

Price, J. D., & Wood, R. (2002). Comparison of probability density functions for total specific humidity and saturation deficit humidity, and consequences for cloud parameterization. *Quarterly Journal of the Royal Meteorological Society*, *128*(584), 2059–2072. <https://doi.org/10.1256/003590002320603539>

Pritchard, M. S., Moncrieff, M. W., & Somerville, R. C. J. (2011). Orographic propagating precipitation systems over the United States in a global climate model with embedded explicit convection. *Journal of the Atmospheric Sciences*, *68*(8), 1821–1840. <https://doi.org/10.1175/2011JAS3699.1>

Randall, D., Khairoutdinov, M., Arakawa, A., & Grabowski, W. (2003). Breaking the cloud parameterization deadlock. *Bulletin of the American Meteorological Society*, *84*(11), 1547–1564. <https://doi.org/10.1175/BAMS-84-11-1547>

Satoh, M., Stevens, B., Judt, F., Khairoutdinov, M., Lin, S.-J., Putman, W. M., & Düben, P. (2019). Global cloud-resolving models. *Current Climate Change Reports*, *5*(3), 172–184. <https://doi.org/10.1007/s40641-019-00131-0>

Seifert, A., & Heus, T. (2013). Large-eddy simulation of organized precipitating trade wind cumulus clouds. *Atmospheric Chemistry and Physics*, *13*(11), 5631–5645. <https://doi.org/10.5194/acp-13-5631-2013>

Siebesma, A. P., Bretherton, C. S., Brown, A., Chlond, A., Cuxart, J., Duynkerke, P. G., et al. (2003). A large eddy simulation intercomparison study of shallow cumulus convection. *Journal of the Atmospheric Sciences*, *60*(10), 1201–1219. [https://doi.org/10.1175/1520-0469\(2003\)60<1201:ALESIS>2.0.CO;2](https://doi.org/10.1175/1520-0469(2003)60<1201:ALESIS>2.0.CO;2)

Sparrow, S., Bowery, A., Carver, G. D., Köhler, M. O., Ollinaho, P., Pappenberger, F., et al. (2021). OpenIFS@home version 1: A citizen science project for ensemble weather and climate forecasting. *Geoscientific Model Development*, *14*(6), 3473–3486. <https://doi.org/10.5194/gmd-14-3473-2021>

Stevens, B., Ackerman, A. S., Albrecht, B. A., Brown, A. R., Chlond, A., Cuxart, J., et al. (2001). Simulations of trade wind cumuli under a strong inversion. *Journal of the Atmospheric Sciences*, *58*(14), 1870–1891. [https://doi.org/10.1175/1520-0469\(2001\)058<1870:SOTWCU>2.0.CO;2](https://doi.org/10.1175/1520-0469(2001)058<1870:SOTWCU>2.0.CO;2)

- Stevens, B., Ament, F., Bony, S., Crewell, S., Ewald, F., Gross, S., et al. (2019). A high-altitude long-range aircraft configured as a cloud observatory: The NARVAL expeditions. *Bulletin of the American Meteorological Society*, *100*(6), 1061–1077. <https://doi.org/10.1175/BAMS-D-18-0198.1>
- Stevens, B., Bony, S., Brogniez, H., Hentgen, L., Hohenegger, C., Kiemle, C., et al. (2020). Sugar, gravel, fish and flowers: Mesoscale cloud patterns in the trade winds. *Quarterly Journal of the Royal Meteorological Society*, *146*(726), 141–152. <https://doi.org/10.1002/qj.3662>
- Stevens, B., Bony, S., Farrell, D., Ament, F., Blyth, A., Fairall, C., et al. (2021). EUREC⁴A. *Earth System Science Data*, *13*(8), 4067–4119. <https://doi.org/10.5194/essd-13-4067-2021>
- Stevens, B., Moeng, C.-H., Ackerman, A. S., Bretherton, C. S., Chlond, A., de Roode, S., et al. (2005). Evaluation of large-eddy simulations via observations of nocturnal marine stratocumulus. *Monthly Weather Review*, *133*(6), 1443–1462. <https://doi.org/10.1175/MWR2930.1>
- Stevens, B., Satoh, M., Auger, L., Biercamp, J., Bretherton, C. S., Chen, X., et al. (2019). DYAMOND: The dynamics of the atmospheric general circulation modeled on non-hydrostatic domains. *Progress in Earth and Planetary Science*, *6*(1), 61. <https://doi.org/10.1186/s40645-019-0304-z>
- Tao, W.-K., Chern, J.-D., Atlas, R., Randall, D., Khairoutdinov, M., Li, J.-L., et al. (2009). A multiscale modeling system: Developments, applications, and critical issues. *Bulletin of the American Meteorological Society*, *90*(4), 515–534. <https://doi.org/10.1175/2008BAMS2542.1>
- Tomita, H. (2008). New microphysical schemes with five and six categories by diagnostic generation of cloud ice. *Journal of the Meteorological Society of Japan. Series II*, *86A*, 121–142. <https://doi.org/10.2151/jmsj.86A.121>
- Tulich, S. N. (2015). A strategy for representing the effects of convective momentum transport in multiscale models: Evaluation using a new superparameterized version of the weather research and forecast model (SP-WRF). *Journal of Advances in Modeling Earth Systems*, *7*(2), 938–962. <https://doi.org/10.1002/2014MS000417>
- van den Oord, G., Jansson, F., Pelupessy, I., Chertova, M., Grönqvist, J. H., Siebesma, P., & Crommelin, D. (2020). A Python interface to the Dutch Atmospheric Large-Eddy Simulation. *Software*, *12*, 100608. <https://doi.org/10.1016/j.softx.2020.100608>
- van Heerwaarden, C. C., van Stratum, B. J. H., Heus, T., Gibbs, J. A., Fedorovich, E., & Mellado, J. P. (2017). MicroHH 1.0: A computational fluid dynamics code for direct numerical simulation and large-eddy simulation of atmospheric boundary layer flows. *Geoscientific Model Development*, *10*(8), 3145–3165. <https://doi.org/10.5194/gmd-10-3145-2017>
- vanZanten, M. C., Stevens, B., Nuijens, L., Siebesma, A. P., Ackerman, A. S., Burnet, F., et al. (2011). Controls on precipitation and cloudiness in simulations of trade-wind cumulus as observed during RICO. *Journal of Advances in Modeling Earth Systems*, *3*(2), 13. <https://doi.org/10.1029/2011MS000056>